IOP Publishing SUPERCONDUCTOR SCIENCE AND TECHNOLOGY

Supercond. Sci. Technol. **26** (2013) 015004 (10pp) doi:10.1088/0953-2048/26/1/015004

Non-equilibrium superconductivity in quantum-sensing superconducting resonators

D J Goldie and S Withington

Detector and Optical Physics Group, Cavendish Laboratory, University of Cambridge, J J Thomson Avenue, Cambridge CB3 0HE, UK

E-mail: d.j.goldie@mrao.cam.ac.uk

Received 30 August 2012, in final form 24 October 2012
Published 8 November 2012
Online at stacks.iop.org/SUST/26/015004

Abstract

Low temperature microwave superconducting resonators (SRs) are attractive candidates for producing quantum-sensitive, arrayable energy or power detectors for astrophysical and other precision measurement applications. Their readout uses a microwave probe signal with quanta of energy well below the threshold for pair-breaking in the superconductor. We have calculated the non-equilibrium quasiparticle and phonon distributions generated by the photons of the probe signal of a resonator operating well below its superconducting transition temperature T_c as the absorbed probe power was changed using the coupled kinetic equations described by Chang and Scalapino. The calculations give insight into a rate equation estimate which suggests that the quasiparticle distributions can be driven far from their thermal equilibrium value for typical readout powers. From the driven quasiparticle distribution functions, the driven quasiparticle number densities and lifetimes were calculated. An effective temperature to describe the driven quasiparticles was defined. The non-equilibrium lifetimes were compared to the distribution-averaged thermal lifetimes at the effective temperature and good agreement was found typically within a few per cent. We used the non-equilibrium quasiparticle distribution to model a representative SR. The complex conductivity and hence the frequency dependence of the experimentally measured forward scattering parameter S_{21} of the SR as a function of absorbed power were found. The non-equilibrium S_{21} cannot be accurately modeled by a thermal distribution even at its own elevated temperature, having a higher quality factor in all cases studied, although for low absorbed powers the two effective temperatures are similar. From the non-equilibrium lifetimes and number densities we determined the achievable noise equivalent power (NEP) of the resonator used as a power detector as a function of absorbed microwave power. Simpler expressions to evaluate the effective quasiparticle temperature as a function of absorbed power have also been derived. We conclude that multiple photon absorption from the microwave probe increases the quasiparticle number above the thermal background and ultimately limits the achievable NEP of the resonator at temperatures well below T_c.

(Some figures may appear in colour only in the online journal)

1. Introduction

Microwave superconducting resonators (SRs) with high quality factor Q operating at low reduced temperatures $T/T_c \simeq 0.1$, where T is the temperature and T_c is the superconducting transition temperature, are used not only as ultra-sensitive detectors of incident power or individual quanta for applications in sub-millimeter, millimeter, optical, x- and γ-ray astrophysics [1–6], but also as elements of Qubits for quantum computing [7–9]. They are also needed as elements of microwave superconducting Quantum interference device (SQUID) multiplexers [10] and also some SQUID geometries more directly. Despite this technological importance, a detailed microscopic analysis of the effect on the distribution functions of the quasiparticles and phonons of the superconducting state at temperatures $T \sim 0.1T_c$ due to the interaction of a *flux* of microwave photons of frequency $\nu_p \ll 2\Delta(T)/h$, where $2\Delta(T)$ is the temperature-dependent superconducting energy gap and h is Planck's constant, seems to be sorely lacking. By contrast the regime $\nu_p \sim \Delta(T)/h$ with $T \sim T_c$, when gap-enhancement effect are predicted and observed, has been extensively studied. The quasiparticles and phonons of a low temperature superconductor form coupled subsystems. Energy relaxation processes of quasiparticles that couple to phonons comprise scattering with absorption or emission of phonons, and scattering involving Cooper pairs with generation or loss of two quasiparticles and absorption or emission of phonons of energy $\Omega \geq 2\Delta$ respectively. Energy escapes from the superconductor as phonons enter the substrate. The coupled kinetic equations that describe these interacting subsystems were derived by Bardeen *et al* [11] and discussed in detail by Chang and Scalapino [12, 13]. In [12] the coupled equations were linearized and solved for a variety of drive sources including microwaves. In [13] full non-linear solutions were obtained. Crucially however in that work solutions were obtained close to T_c where microwave drive can lead to gap-enhancement effects. The same kinetic equations have also been used to investigate the non-linear effect of high-energy photon interactions at $T/T_c \sim 0.1$ [14–16].

It could be assumed that if $h\nu_p < 2\Delta$ the photon interaction will not change the quasiparticle number since the photon cannot break a Cooper pair. Whilst true at the single quantum level, this assumption ignores the effect of a flux of photons which might be used in a typical experiment and the competing effects of multiple photon absorption against single quasiparticle scattering or recombination on the driven quasiparticle distribution $f(E)$ where E is the energy. Indeed the effect of the microwave probe on the SR may already have been observed [6]. Understanding the effect of non-equilibrium quasiparticles on a Qubit is certainly a topic of current interest [17, 18], where non-equilibrium quasiparticles may be a limiting factor on Qubit energy relaxation times. Our interest is particularly in the context of non-equilibria in SRs used as precision power or quantum-sensing detectors although we would emphasize that our calculations apply to SRs in general and the mechanisms and solutions we describe are common to all SR applications. Indeed the results presented below are *independent* of the particular geometry or application provided the effect of geometry on the power absorbtion is considered. In this report we ignore the effect of critical current on the SR, indeed our estimates indicate that, even at the highest powers considered, the SR response is not be limited by its critical current.

In the context of power measurement or quantum spectroscopy, SRs are sensitive to changes in incident energy because of the dependence of the surface impedance Z_s of the superconductor on quasiparticle density and the dependence follows from the complex conductivity σ described by Mattis and Bardeen [19]. The SR is embedded in an electrical readout circuit and is driven by a microwave probe signal of frequency $\nu_p \sim 0.1\Delta(T)/h$ close to the circuit resonant frequency ν_0. If the quasiparticle density is changed, for example by absorption of a photon of sufficient energy to break Cooper pairs directly $h\nu_\Phi > 2\Delta$, where ν_Φ is the detected photon frequency, Z_s is changed and the change can be monitored by measuring the change in the (complex) resonance transmission characteristic $S_{21}(\nu)$ of the probe signal. The change relaxes back to the unperturbed state as energy is exchanged between the quasiparticles and the phonons of the superconductor and ultimately the substrate. In this way very sensitive power or energy detectors can be made. For example [6] estimated a dark noise equivalent power (NEP), i.e. ignoring the achieved signal detection efficiency, of 2×10^{-19} W Hz$^{-1/2}$ at lowest readout power which was accounted for in terms of the generation–recombination noise of the quasiparticles and a limiting lifetime of 3–4 ms, and it has been suggested that NEP's of order 10^{-20} W Hz$^{-1/2}$ may be achieve [20]. The readout naturally lends itself to frequency-division multiplexing where a large number of SRs each operating with a slightly different ν_0 are coupled to a through-transmission line. A high Q resonator can be formed by lithographically patterning a low-T_c superconducting thin film such as Al ($T_c = 1.2$ K) on a dielectric substrate. The substrate is held at the bath temperature $T = T_b$. A number of SR geometries are possible including ring, half- and quarter-wave or lumped-element designs.

In a recent paper we discussed the effect of the probe power on the resonator characteristic [21]. The key point is that the readout is dissipative [2, 6, 22] and the absorbed probe power can be calculated knowing the embedding electrical circuit. Probe photons are absorbed by the quasiparticles of the SR which changes $f(E)$, although the resulting distribution has not yet been calculated. In a real device other mechanisms may contribute to the dissipation for example dielectric or radiative losses [2]. Here we focus on the dissipation associated with the real part of σ. The aim of this work is to calculate the effect of a microwave drive at low temperatures ($T_b/T_c = 0.1$) on the static, non-equilibrium quasiparticle and phonon distributions the SR as the probe power levels are changed. We also derive simpler analytical expressions which give a good approximation to the key results of the full calculation.

The structure of this paper is as follows. In section 2 we give an estimate of the power densities where non-equilibrium effects are likely to become important in a SR. In section 3 we discuss the general properties of the coupled kinetic equations and derive the form for the drive and subsystem power flow terms necessary to ensure energy conservation whilst also discussing the effects of out-diffusion in a real geometry and the method used to calculate distribution-averaged recombination times. In section 4 we give numerical parameters used in calculations to describe a clean thin-film superconductor (Al), and in section 4.1 we describe the model used to calculate S_{21} for a representative SR. Section 5 describes the numerical method. In section 6 we show solutions for the non-equilibrium quasiparticle and phonon distributions of a driven SR operating with $T_b/T_c = 0.1$ as a function of P_{abs} including calculations of driven quasiparticle density N_{qp}, an effective temperature T_N^* determined from N_{qp}, and of the distribution-averaged relaxation time τ_r. We calculate the driven S_{21} for a representative Al SR under the same powers. We also estimate the effect on the achievable NEP for a quantum SR detector using these results. Section 7 describes two models both giving a reasonable but numerically simpler account of the results. In section 8 we discuss the implications of the work with concluding remarks.

2. Equilibrium estimate

In this section we use the equilibrium interaction times derived by Kaplan *et al* [23] to estimate the power densities where non-equilibrium effects are likely to occur in a SR at low temperatures. Reference [23] gives expressions for the thermal equilibrium lifetimes: $\tau_s(E, T)$ for the scattering of quasiparticles of energy E, $\tau_r(E, T)$ for recombination to Cooper pairs, $\tau_{\phi s}(\Omega, T)$ for the scattering of phonons of energy Ω and $\tau_{pb}(\Omega, T)$ for a phonon to break a pair. These are calculated in terms of characteristic quasiparticle and phonon lifetimes τ_0 and τ_0^ϕ. The volume density of thermal quasiparticles is $N(T) = 4N(0)\int_\Delta^\infty \rho(E, \Delta(T))f(E, T)\,\mathrm{d}E$, where $\rho(E, \Delta) = E/\sqrt{E^2 - \Delta^2}$ is the normalized quasiparticle density of states, $f(E, T) = (\exp(E/k_bT) + 1)^{-1}$ is the Fermi distribution at temperature T (in contrast to $f(E)$ the driven distribution), k_b is Boltzmann's constant and $N(0)$ is the single-spin density of states at the Fermi energy. Consider the case of an Al resonator with a probe signal of $\nu_p \sim 4$ GHz. Since $h\nu_p \simeq 2\Delta/20$ it is not clear that the probe signal is capable of changing the equilibrium $N(T)$ and hence $\Delta(T)$. Our measurements and modeling show that typical experimental readout powers dissipate of order $1 \to 100$ aW μm^{-3} in an Al SR used as a power detector [3, 21].

The probe photons are absorbed by the quasiparticles changing their energy distribution $f(E)$. We expect the appearance of at least one peak in $f(E)$ around $E = h\nu_p$ due to absorption of the monochromatic probe photons by the large density of quasiparticles near to the gap, perhaps more peaks if P_{abs} is sufficiently high. Assume that energy relaxation of an excited quasiparticle can only occur by scattering with emission of phonons and all of the emitted phonons are lost from the film with an energy-independent time τ_l. Indeed, for thermal distributions at low reduced temperatures quasiparticle-scattering times are significantly shorter than recombination times [23]. However if $f(E)$ has *any* non-equilibrium quasiparticles above $E = 3\Delta$ the phonon emitted in scattering may have $\Omega > 2\Delta$ which can break a pair. This is the onset of non-equilibrium effects since the number of quasiparticles can be changed. We can obtain a naive estimate of the probe power level for this to occur by assuming that all of the available quasiparticles at T_b i.e. $N(T) \equiv N(T_b)$, are driven to the same (to be determined) energy E_δ and that scattering is the only energy loss mechanism for the quasiparticles, so

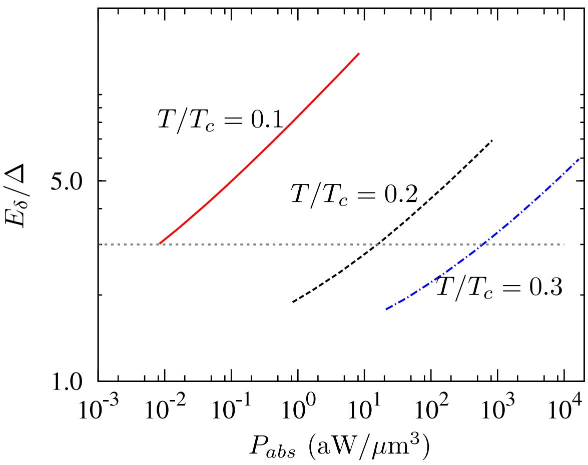

Figure 1. Quasiparticle energy E_δ as a function of P_{abs} for an Al film at 3 bath temperatures assuming cooling by quasiparticle-phonon scattering alone.

that $P_{abs} = E_\delta N(T_b)/\tau_s(E_\delta, T_b)$. Figure 1 shows E_δ for three bath temperatures as a function of P_{abs} calculated for an Al film with $\Delta(0) = 180$ μeV, $T_c = 1.17$ K, $N(0) = 1.74 \times 10^4$ μeV^{-1} μm^{-3}, and $\tau_0 = 438$ ns. At $T_b/T_c = 0.1$ all the quasiparticles would have $E_\delta > 3\Delta$ for these P_{abs} and then the phonon emitted in scattering could break a pair. Even at $T_b/T_c = 0.2$, E_δ is close to the pair-breaking threshold. We would note that this estimate is probably conservative: non-equilibrium effects occur as soon as there are any non-thermal quasiparticles with $E \geq 3\Delta$ and the degree of non-equilibrium depends on the probability of pair-breaking before loss by the scattered phonons, τ_l/τ_{pb}. At low temperatures $\tau_{pb} = \tau_0^\phi$. For a 100 nm Al film on sapphire or Si we estimate that $\tau_l \sim \tau_{pb}$ [24]. This suggests that the probe signal may break Cooper pairs in the driven SR even for very low P_{abs} and scattering without pair-breaking may not be a sufficient energy relaxation mechanism. Then a full non-equilibrium description is required and we will not be surprised if the power densities to observe non-equilibrium effects may be lower than suggested by figure 1.

3. Non-equilibrium resonators

In this and subsequent sections we describe and use a full non-linear solution of the kinetic equations for the coupled quasiparticle and phonon systems. The rates of change of the distribution functions, $f(E)$ for the quasiparticles and $n(\Omega)$ for the phonons, are given in equations (7) and (8) of [13]. Substituting τ_0 and τ_0^ϕ these become

$$\frac{\mathrm{d}f(E)}{\mathrm{d}t} = I_{qp}(E, \nu_p) - \frac{1}{\tau_0(k_bT_c)^3}\int_0^\infty \mathrm{d}\Omega\,\Omega^2\rho(E+\Omega) \times \left(1 - \frac{\Delta^2}{E(E+\Omega)}\right) \times (f(E)[1 - f(E+\Omega)]n(\Omega) - [1 - f(E)]f(E+\Omega)[n(\Omega)+1]) - \frac{1}{\tau_0(k_bT_c)^3}\int_0^{E-\Delta} \mathrm{d}\Omega\,\Omega^2\rho(E-\Omega)$$

$$\times\left(1-\frac{\Delta^2}{E\,(E-\Omega)}\right)$$
$$\times\,(f\,(E)\,[1-f\,(E-\Omega)]\,[n\,(\Omega)+1]$$
$$-\,[1-f\,(E)]f\,(E-\Omega)\,n\,(\Omega))$$
$$-\,\frac{1}{\tau_0(k_{\rm b}T_{\rm c})^3}\int_{E+\Delta}^{\infty}{\rm d}\Omega\,\Omega^2\rho(\Omega-E)$$
$$\times\left(1+\frac{\Delta^2}{E\,(\Omega-E)}\right)(f\,(E)f\,(\Omega-E)$$
$$\times\,[n\,(\Omega)+1]-[1-f\,(E)]$$
$$\times\,[1-f\,(\Omega-E)]\,n\,(\Omega)), \tag{1}$$

and

$$\frac{{\rm d}n(\Omega)}{{\rm d}t}=-\frac{2}{\pi\tau_0^{\phi}\Delta(0)}\int_{\Delta}^{\infty}{\rm d}E\,\rho(E)\rho(E+\Omega)$$
$$\times\left(1-\frac{\Delta^2}{E\,(E+\Omega)}\right)$$
$$\times\,(f\,(E)\,[1-f\,(E+\Omega)]\,n\,(\Omega)$$
$$-\,[1-f\,(E)]f\,(E+\Omega)\,[n\,(\Omega)+1])$$
$$-\,\frac{1}{\pi\tau_0^{\phi}\Delta(0)}\int_{\Delta}^{\Omega-\Delta}{\rm d}E\,\rho(E)\rho(\Omega-E)$$
$$\times\left(1+\frac{\Delta^2}{E\,(\Omega-E)}\right)([1-f\,(E)]$$
$$\times\,[1-f\,(\Omega-E)]\,n\,(\Omega)-f\,(E)f\,(\Omega-E)$$
$$\times\,[n\,(\Omega)+1])-\frac{n(\Omega)-n(\Omega,T_{\rm b})}{\tau_l}, \tag{2}$$

where $n(\Omega, T_{\rm b}) = (\exp(\Omega/k_{\rm b}T_{\rm b}) - 1)^{-1}$ is the Bose distribution evaluated at $T_{\rm b}$. The term $I_{\rm qp}(E, \nu_{\rm p})$ is the source term due to the photons at energy E and quantifies the drive of the microwave probe. The energy gap is modified from its equilibrium value and is determined self-consistently so that

$$\frac{1}{N(0)V_{\rm BCS}}=\int_{\Delta}^{\infty}{\rm d}E\,\frac{1-2f(E)}{\sqrt{E^2-\Delta^2}}, \tag{3}$$

where $V_{\rm BCS}$ is the BCS interaction parameter. Equation (3) calculates the non-equilibrium Δ using the non-equilibrium $f(E)$. In the static, driven situation to be solved ${\rm d}f(E)/{\rm d}t = {\rm d}n(\Omega)/{\rm d}t = 0$.

3.1. Microwave drive term

The form of $I_{\rm qp}(E, h\nu_{\rm p})$ was calculated by Eliashberg *et al* [25, 26] and

$$I_{\rm qp}(E,\nu_{\rm p})=2{\rm B}\left[\rho(E+h\nu_{\rm p},\Delta)\left[1+\frac{\Delta^2}{E\,(E+h\nu_{\rm p})}\right]\right.$$
$$\times\,\left[f\,(E+h\nu_{\rm p})-f\,(E)\right]$$
$$-\,\rho(E-h\nu_{\rm p},\Delta)\left[1+\frac{\Delta^2}{E\,(E-h\nu_{\rm p})}\right]$$
$$\left.\times\,\left[f\,(E)-f\,(E-h\nu_{\rm p})\right]\right] \tag{4}$$

where the rate coefficient B needs to be determined for low temperatures. A third term arises in equation (4) if $h\nu_{\rm p} \geq 2\Delta$,which is not considered here since we are investigating the effect of sub-gap photons. Equation (4) describes both absorption and emission of single photons. Reference [12] used a different rate coefficient to describe the interaction of microwaves at normal incidence to a superconducting film close to $T_{\rm c}$ which, in our notation, would be $B' \propto H^2R_{\rm n}/dN(0)\nu^2$ with H the magnetic field strength, $R_{\rm n}$ the *normal-state* square sheet resistance and d the film thickness. For a SR at $T/T_{\rm c} = 0.1$ the field does not interact with a normal-state metal in that geometry, neither is the penetration of the field into the superconductor determined by the normal-state parameter. We take a different approach which emerges naturally by considering energy conservation. Assuming uniform absorption, the power absorbed per unit volume of the resonator is

$$P_{\rm abs}=4N(0)\int_{\Delta}^{\infty}{\rm d}E\,I_{\rm qp}(E,\nu_{\rm p})E\rho(E,\Delta). \tag{5}$$

We solve equations (1) and (2) numerically so that writing $I_{\rm qp}(E, \nu_{\rm p}) = {\rm B}K_{\rm qp}(E, \nu_{\rm p})$ we can also include a power absorption error term

$$\delta P=4N(0){\rm B}\int_{\Delta}^{\infty}{\rm d}E\,K_{\rm qp}(E,\nu_{\rm p})E\rho(E,\Delta)-P_{\rm abs}, \tag{6}$$

where B needs to be determined to satisfy this equation, and the static non-equilibrium solution sought is $\delta P = 0$.

3.2. Quasiparticle-phonon power

The power flow from the quasiparticles to the phonons can be found by recognizing that the sum of the integrals on the right-hand-side of equation (1) gives the total rate of change of $f(E)$ due to interactions with phonons, $I_{\text{qp-}\phi}(E)$. The energy leaving the quasiparticles per unit volume per unit time is

$$P_{\text{qp-}\phi}=4N(0)\int_{\Delta}^{\infty}{\rm d}E\,I_{\text{qp-}\phi}(E)E\rho(E,\Delta). \tag{7}$$

We define the fractional quasiparticle-phonon power flow error term

$$\xi_{\text{qp-}\phi}=\frac{P_{\rm abs}-P_{\text{qp-}\phi}}{P_{\rm abs}}. \tag{8}$$

3.3. Phonon cooling term

Energy is lost from a SR as non-equilibrium phonons are lost into the substrate. The energy leaving the phonons per unit volume of the film per unit time is given by

$$P_{\phi-b}=\sum_{br}N_{\rm ion}\int_0^{\infty}{\rm d}\Omega\,D(\omega)\Omega\frac{n(\Omega)-n(\Omega,T_{\rm b})}{\tau_l}. \tag{9}$$

With a Debye model the density of states is given by $D(\omega) = 3\Omega^2/\Omega_{\rm D}^3$, $\Omega_{\rm D}$ is the Debye energy, and the sum over the phonon branches introduces an additional factor of three. We define a further error term

$$\xi_{\phi-b}=\frac{P_{\rm abs}-P_{\phi-b}}{P_{\rm abs}}. \tag{10}$$

Equations (8) and (10) provide an important monitor of the accuracy of the numerical solutions to the coupled equations.

3.4. Power absorption and the effect of geometry

Power absorption in a resonator is dependent on its geometry and we assumed P_{abs} was known. In modeling, we assumed that probe photons were uniformly absorbed in the SR. Quasiparticle diffusion lengths for clean superconducting films are relatively long ensuring that power absorption with respect to the thickness or width of a typical SR satisfy this assumption. In practice geometric effects associated with the length of the SR should be accounted for and these depend on the particular realization. For example a $\lambda/4$-resonator is a useful geometry into which to couple an external pair-breaking signal. The longitudinal current density distribution in this device is described by $J(x) = J(x_0)\sin(\pi x/2x_0)$, which is a maximum $J(x_0)$ at the shorted end $x = x_0$, and the peak power density is a factor close to two-times higher than the average. For the same reason, as a detector the $\lambda/4$-SR is most sensitive to changes in the quasiparticle density at its shorted end. Mirror currents in the ground-plane mean that the effective volume for the power absorption is up to twice that of the central conductor. However when using a $\lambda/4$ resonator as a detector out-diffusion of the excess quasiparticles generated by the in-coming signal itself must be minimized in order to maximize the detection sensitivity, which may be achieved for example using a higher energy gap contact to the electrical ground. For a $\lambda/2$-SR out-diffusion from the central volume cannot occur. To make our model most general, we ignored out-diffusion of quasiparticles. In practice other resonator geometries can be used and the effect of geometry and out-diffusion on power absorption can in principle be calculated.

3.5. Recombination times

In what follows we calculated distribution-averaged quasiparticle recombination times τ_r for the driven $f(E)$. We used [12] equation (A9) to find the rate coefficient R averaged over $f(E)$ and set $\tau_r = (2RN_{\mathrm{qp}})^{-1}$ with $N_{\mathrm{qp}} = 4N(0)\int_\Delta^\infty \mathrm{d}E\,\rho(E)f(E)$ the non-equilibrium quasiparticle density. If the detected power is small compared to the probe power this is the appropriate measure of the small-signal relaxation time. For a thermal distribution we find $\tau_r \equiv \langle\tau_r(T)\rangle_{\mathrm{qp}}$, the distribution-averaged recombination time described by Kaplan *et al.*

4. Numerical parameters

To describe the resonator we used material parameters appropriate for Al with $N(0)V_{\mathrm{BCS}} = 0.167$ giving $\Delta(0) = 180\ \mu\mathrm{eV}$, $T_c = 1.17$ K and we set $T_b/T_c = 0.1$. We used $N(0) = 1.74\times10^4\ \mu\mathrm{eV}^{-1}\ \mu\mathrm{m}^{-3}$, $\tau_0 = 438$ ns and $\tau_0^{\mathrm{ph}} = 0.26$ ns [23]. The latter was calculated assuming that the appropriate value for the phonon density of states in the calculation of τ_0^{ph} is α_D^2 appropriate for a Debye model as given in table II of [23], an approach suggested in [14]. To be precise, in our view the parameters needed as inputs for modeling are not collectively and with sufficient precision known from measurement or theory. Considering the pre-factors in equations (1), (2), (7) and (9), we found that the numerical inputs must satisfy

$$\frac{2\pi N(0)\tau_0^{\phi}\Delta_0\Omega_D^3}{9N_{\mathrm{ion}}\tau_0\,(k_b T_c)^3} = 1 \tag{11}$$

to allow a self-consistent solution where the power errors equations (8) and (10) converged to zero.

4.1. Parameters for a $\lambda/4$-resonator

In calculations discussed later and shown in figure 7 we investigated the effect of the driven $f(E)$ on a representative device modeling a $\lambda/4$ microstrip resonator as in [21]. The complex conductivity σ which is proportional to the normal-state conductivity σ_N was calculated from equations (3.9) and (3.10) of [19] but using the non-equilibrium $f(E)$. The surface impedance was calculated from σ hence the propagation constant and the characteristic impedance of the SR. The modeled SR had a length of 7.6 mm, width 3 μm, film thickness of 200 nm, dielectric thickness of 200 nm with $\epsilon_r = 3.8$ and a saturation quality factor of 10^7. We set the coupling capacitance to be 5 fF and $\sigma_N = 1.25\times10^8\ (\Omega\ \mathrm{m})^{-1}$, which would be typical for a clean Al film at low temperatures. We calculated a resonant frequency $\nu_0 = 3.934\,21$ GHz ($h\nu_0 = 16.2\ \mu\mathrm{eV}$) with zero absorbed power.

5. Numerical method

A non-equilibrium solution for $f(E)$ and $n(\Omega)$ requires simultaneous solutions of equations (1), (2), (3) and (5). The task is complicated since, for example, equation (1) contains terms such as $f(E\pm\Omega)$ and likewise (6) requires knowledge of $f(E\pm h\nu_p)$, and there are likely to be peaks in the driven distributions arising from the high density of states of quasiparticles near $E = \Delta$.

Equations (1), (2) and (5) were solved using Newton's method. We discretized the distributions $f(E)$ and $n(\Omega)$ using a 1 μeV grid with $E_i = \Delta + i - 1$, $\Omega_i = i$ and $i \in 1\ldots N$ with $N = 1000$ so that quasiparticle states up to $\sim 6.5\Delta(0)$ are considered. We formed the state vector $\boldsymbol{\alpha} = [f_i, \mathrm{B}, n_i]^{\mathrm{T}}$ where T denotes the transpose. We formed the error vector $\boldsymbol{\epsilon} = [\mathrm{d}f_i/\mathrm{d}t, \delta P, \mathrm{d}n_i/\mathrm{d}t]^{\mathrm{T}}$. The iterative procedure seeks to find $\boldsymbol{\epsilon}^{l+1} = 0$ using $\boldsymbol{\alpha}^{l+1} = \boldsymbol{\alpha}^l - \chi\left[\boldsymbol{J}(\boldsymbol{\alpha}^l)\right]^{-1}\boldsymbol{\epsilon}(\boldsymbol{\alpha}^l)$ where the matrix $\boldsymbol{J} = \mathrm{d}\epsilon_j/\mathrm{d}\alpha_k$ is the Jacobian of the partial derivatives and $j, k \in 1\ldots 2N+2$. Analytical expressions for the derivatives can be found making the Jacobian efficient to evaluate. The superscript l denotes the iteration number. $\chi \le 1$ is a convergence parameter and we find $0.8 \le \chi \le 0.95$ gives reasonably rapid convergence typically within 10 iterations.

We assumed a starting thermal $f^0 = f(E_i, T_{\mathrm{start}})$ with an initial temperature $T_{\mathrm{start}} \sim 2T_b$ The value chosen for T_{start} did not affect the solutions obtained merely the number of iterations required to converge sufficiently. Using an earlier estimate of the non-equilibrium distributions reduces the

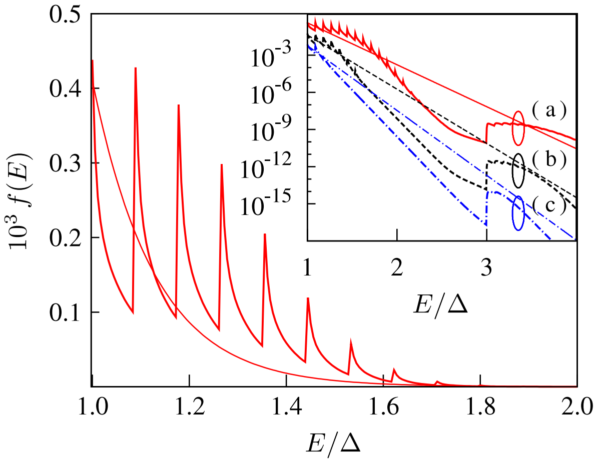

Figure 2. Non-equilibrium distribution for absorbed power 2 fW $\mu\mathrm{m}^{-3}$ with $T_\mathrm{b}/T_\mathrm{c} = 0.1$ and $\tau_l/\tau_\mathrm{pb} = 1$. The continuous curve is a Fermi distribution $f(E, T_\mathrm{N}^*)$ having the same quasiparticle density. The inset shows semi-log plots for powers of (a) 2 fW $\mu\mathrm{m}^{-3}$ (full), (b) 20 aW $\mu\mathrm{m}^{-3}$ (dashed) and (c) 0.2 aW $\mu\mathrm{m}^{-3}$ (dot–dash). The associated straight lines, with the same line styles, show the thermal distributions having the same number density of quasiparticles as the driven $f(E)$ in each case.

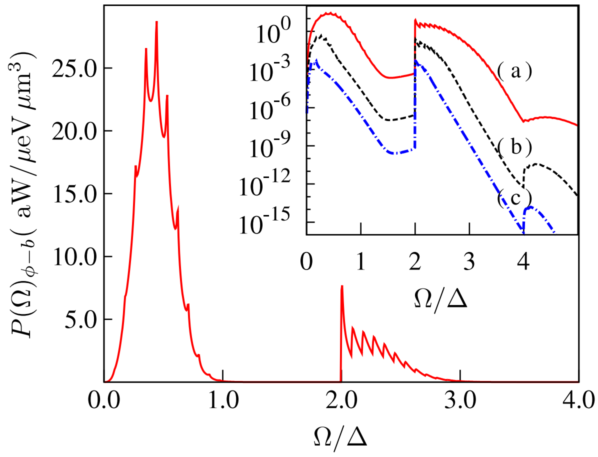

Figure 3. Contributions to the phonon power flow for absorbed power 2 fW $\mu\mathrm{m}^{-3}$. The inset shows semi-log plots for absorbed powers of (a) 2 fW $\mu\mathrm{m}^{-3}$, (b) 20 aW $\mu\mathrm{m}^{-3}$ and (c) 0.2 aW $\mu\mathrm{m}^{-3}$. all with $\tau_l/\tau_\mathrm{pb} = 1$.

number of iterations (or increases the precision for the same computation time) and is a useful approach if parameters such as power or phonon-trapping factors are being varied systematically. We chose $n^0 = n(\Omega_i, T_\mathrm{b})$ so that the phonons are initially at the bath temperature. The aim was to find $f^l(E)$ and $n^l(\Omega)$ such that $|\xi^l_{\mathrm{qp}\text{-}\phi}|, |\xi^l_{\phi-b}| \leq 0.1\%$ for both power transfer error terms. All solutions shown below exceed these convergence criteria in some cases by nearly an order of magnitude. For the microwave drive we restricted ν_p to match the discretized distributions. This means that the onset of any photon induced peaks occurs in well-defined bins of both $f(E_i)$ and $n(\Omega_i)$.

We found that in our solutions the non-equilibrium gap calculated with equation (3) changed very little from $\Delta(T_\mathrm{b})$ and by a maximum of $\delta\Delta \sim 50$ nV. For this reason we did not allow Δ to change in the simulations. The exception to this was for calculations of S_{21} shown later in figure 7. S_{21} is very sensitive to the value of Δ used in the calculation of the conductivity. In this case we linearly interpolated $f(E)$ to find self-consistent values for the non-equilibrium gap $\Delta(f(E))$ using equation (3) which was used to calculate S_{21}. The numerical solutions are slightly sensitive to the grid used due to the approximation involved in representing the large density of states near the gap. We found that the 1 μeV grid with a gap function $\rho(E) = \mathrm{Re}(E/\sqrt{E^2 - (\Delta + 0.001\Delta \mathrm{i})^2})$ to account for physical gap-smearing gave a reasonable representation of the density of states.

6. Solutions for non-equilibrium resonators

In this section we show results of the modeling. Figure 2 shows $f(E)$ with $\nu_\mathrm{p} = 3.8804$ GHz ($h\nu_\mathrm{p} = 16$ μeV), which is close to ν_0 for the $\lambda/4$-Al SR that we later use as an example, with $T/T_\mathrm{c} = 0.1$, $P_\mathrm{abs} = 2$ fW $\mu\mathrm{m}^{-3}$ and $\tau_l/\tau_\mathrm{pb} = 1$. The multi-peaked structure is consistent with sequential single photon absorption; the drive term of equation (4) only describes single photon events. The occurrence of this multi-peaked structure is expected if the SR is driven far from equilibrium. Pleasingly this structure emerges in the very first iteration of the numerical method. In addition physically unrealistic distributions (where for example $f(E - h\nu) < f(E)$ at $E < 3\Delta$) were never found. Figure 2 includes a thermal distribution $f(E, T_\mathrm{N}^*)$ where T_N^* is defined so that $4N(0)\int_\Delta^\infty f(E, T_\mathrm{N}^*)\rho(E)\,\mathrm{d}E = N_\mathrm{qp}$ i.e. the thermal distribution having the same number density of quasiparticles as the driven case. The non-equilibrium nature of $f(E)$ becomes further apparent in the semi-log plots in the inset which are calculated for P_abs of (a) 2 fW $\mu\mathrm{m}^{-3}$, (b) 20 aW $\mu\mathrm{m}^{-3}$ and (c) 0.2 aW $\mu\mathrm{m}^{-3}$ where the presence of quasiparticles with $E \geq 3\Delta$ also showing multiple photon induced structure can be seen. These quasiparticles arise from absorption of 2Δ-phonons by quasiparticles. A further much-reduced feature (not plotted) at $E \geq 5\Delta$ is also found. A recurring feature of these solutions is that the driven low-energy $f(E)$ shows excess densities of quasiparticles at energies of order $E < \Delta + 10h\nu_\mathrm{p}$ above the equivalent T_N^* distributions (the dashed lines). The effect of this distortion is to increase the power carried by low-energy phonons $\Omega < 2\Delta$ by scattering compared to a thermal distribution and these phonons are more easily lost from the SR providing an efficient cooling mechanism. The distortion from the equivalent thermal distribution increases as P_abs increases, as does the number of photon peaks. At energies $E \sim 3\Delta - 5h\nu_\mathrm{p}$ the calculated $f(E)$ is increased from the by-eye straight line and at the same time for $E \geq 3\Delta$ it is indeed the case that $f(E - h\nu) < f(E)$ for some E. The magnitude of both effects are power dependent, which arises from the competing contributions of non-equilibrium 2Δ-phonon re-absorption and the stimulated *emission* of photons inherent in equation (4).

Figure 3 shows the corresponding contributions to the phonon-bath power flow integral of equation (9), $P(\Omega)_{\phi-b}$,

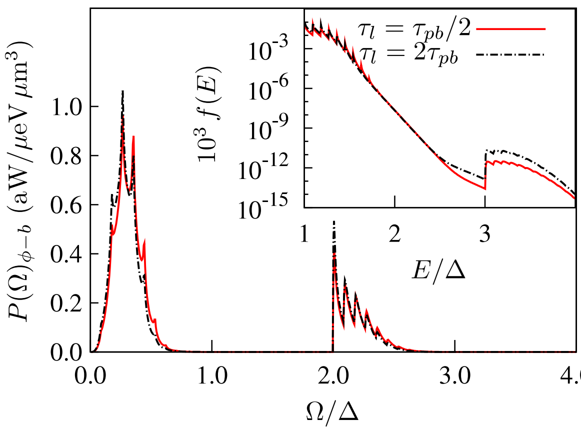

Figure 4. Contributions to the phonon power to the bath $P(\Omega)_{\phi-b}$ and inset the associated $f(E)$ for $P_{\rm abs} = 50$ aW μm^{-3}, $T_{\rm b}/T_{\rm c} = 0.1$, for two values of $\tau_l/\tau_{\rm pb} = 0.5$ (full lines) and 2 (dash–dot lines) with $\tau_l/\tau_{\rm pb} = 1$.

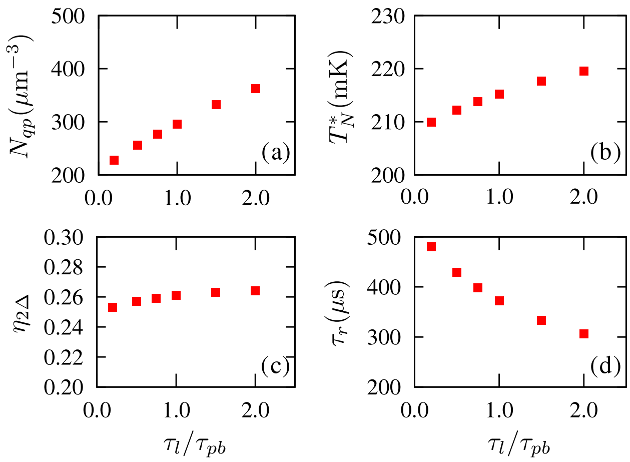

Figure 5. The effect of $P_{\rm abs} = 50$ aW μm^{-3} as a function of $\tau_l/\tau_{\rm pb}$: (a) quasiparticle density, (b) effective temperature $T^*_{\rm N}$, (c) fraction of power carried by 2Δ-phonons and (d) Recombination time for the non-equilibrium $f(E)$.

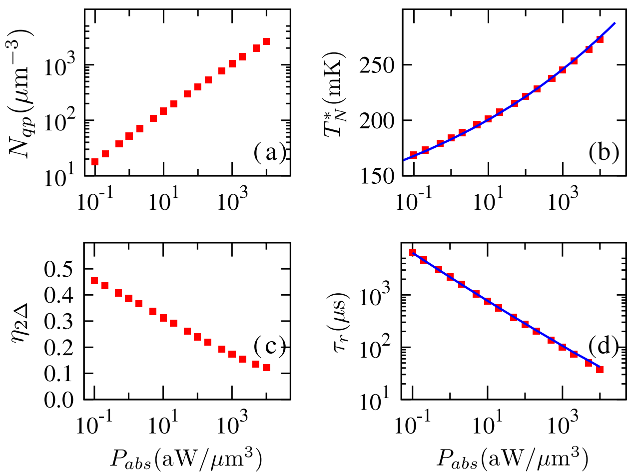

Figure 6. The effect of absorbed power with $\tau_l/\tau_{\rm pb} = 1$: (a) quasiparticle density, (b) effective temperature $T^*_{\rm N}$, (c) fraction of power carried by 2Δ-phonons and (d) recombination time for the non-equilibrium $f(E)$. The full curve in (b) is an analytical expression. The full curve in (d) is the distribution-averaged thermal recombination time $\langle\tau_r(T^*_{\rm N})\rangle_{\rm qp}$.

for the same drive conditions where the presence of non-equilibrium 2Δ-phonons is seen. An additional feature at $\Omega = 4\Delta$ is also found. There are two distinct contributions to $P(\Omega)_{\phi-b}$. At low energies we see phonons arising from the scattering of low-energy quasiparticles towards the gap, and there is structure consistent with the peaks in $f(E)$. Structure on the low-energy side of the phonon peaks is also seen which is expected as the driven $f(E)$ scatters to lower energies and the rate of this scattering is reduced by the occupation of the final states by the driven distribution itself, despite the increasing phonon density of states that would be available for the scattering to occur. At $\Omega \geq 2\Delta$ we see a second distinct contribution to $P(\Omega)_{\phi-b}$. This power is transferred to the substrate by pair-breaking phonons with $\Omega \geq 2\Delta$, which are generated not just by recombination of the excess $f(E)$ itself but also by the scattering (and recombination) of those quasiparticles with $E \geq 3\Delta$. To quantify the fraction of the power carried by phonons with $\Omega \geq 2\Delta$ we define $\eta_{2\Delta} = \int_{2\Delta}^{\infty} {\rm d}\Omega\,(n(\Omega) - n(\Omega, T_{\rm b}))/\int_0^{\infty} {\rm d}\Omega\,(n(\Omega) - n(\Omega, T_{\rm b}))$. In the main plot of figure 3, $\eta_{2\Delta} = 0.16$. Figure 4 shows contributions to $P(\Omega)_{\phi-b}$ for two values of $\tau_l/\tau_{\rm pb}$. Somewhat counter-intuitively increasing $\tau_l/\tau_{\rm pb}$ increases the contribution at the lowest Ω to $P(\Omega)_{\phi-b}$ whilst simultaneously increasing the contribution from pair-breaking phonons $\Omega \geq 2\Delta$. The effect on $f(E)$ is evident in the inset. As $\tau_l/\tau_{\rm pb}$ is increased more 3Δ quasiparticles are generated, these in turn generate more pair-breaking phonons which can be re-absorbed before being lost from the film. Figure 5 shows the effect of changing $\tau_l/\tau_{\rm pb}$ on $N_{\rm qp}$, $T^*_{\rm N}$, $\eta_{2\Delta}$, and τ_r for $P_{\rm abs} = 50$ aW μm^{-3}. Increasing $\tau_l/\tau_{\rm pb}$ increases both $N_{\rm qp}$ and $T^*_{\rm N}$ while τ_r is reduced. In combination this increases the relative contribution of the recombination phonons to the power flow to the bath despite the increasing probability of re-absorption, and for this reason $\eta_{2\Delta}$ increases somewhat. We find that for fixed power the solutions are related by $N_{\rm qp}/\tau_r(1 + \tau_l/\tau_{\rm pb}) = k$ where k is a constant independent of $\eta_{2\Delta}$ although we emphasize that both $N_{\rm qp}$ and τ_r are driven non-equilibrium values.

Figure 6 shows the effect at $T/T_{\rm c} = 0.1$ of varying $P_{\rm abs}$ on $N_{\rm qp}$, $T^*_{\rm N}$, $\eta_{2\Delta}$ and τ_r. Figure 6(a) shows that, for all $P_{\rm abs}$, $N_{\rm qp}$ exceeds the undriven thermal density calculated at $T_{\rm b}$ and, to emphasize, for $T_{\rm b}/T_{\rm c} = 0.1$ we calculate $N_{\rm qp} = 0.1$ μm^{-3}. Readout power significantly changes the driven, static $N_{\rm qp}$. Figure 6(b) shows that $T^*_{\rm N}$ is enhanced above $T_{\rm b}$ for all readout powers studied. The full curve shown is an analytical expression described later in section 7. The distortion of $f(E)$ from even the nearest thermal distribution as $P_{\rm abs}$ is increased means that $\eta_{2\Delta}$ shown in figure 6(c) is also a function of $P_{\rm abs}$. At the lowest powers studied $P_{\rm abs} \sim 0.1$ aW μm^{-3} much of the power leaving the film is carried by recombination phonons, which is as expected given our earlier estimate showing the inefficiency of scattering in the energy relaxation. As $P_{\rm abs}$ is increased $\eta_{2\Delta}$ is reduced and more power is carried by $\Omega < 2\Delta$-phonons emitted

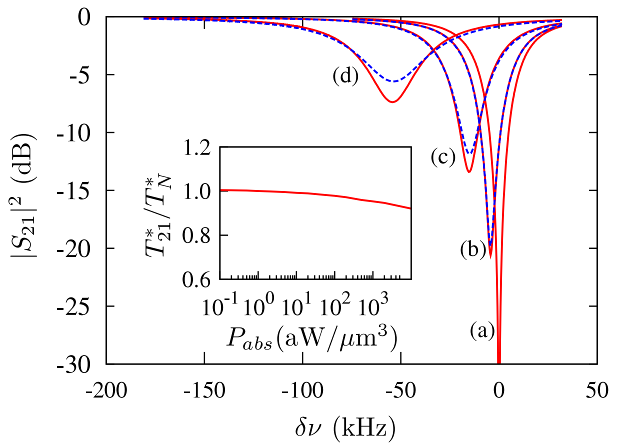

Figure 7. The effect of absorbed power on S_{21} (full lines) with $\tau_l/\tau_{\mathrm{pb}} = 1$ and (dashed lines) the transmission calculated for the nearest thermal distribution $f(E, T^*_{21})$ giving the same resonant frequency: (a) $P_{\mathrm{abs}} = 0$ at T_{b}, (b) $P_{\mathrm{abs}} = 0.1$ aW μm^{-3}, (c) $P_{\mathrm{abs}} = 2$ aW μm^{-3} and (d) $P_{\mathrm{abs}} = 50$ aW μm^{-3}. $\delta\nu$ is referenced to ν_0 with $P_{\mathrm{abs}} = 0$. The inset shows the ratio of T^*_{21} to T^*_{N}.

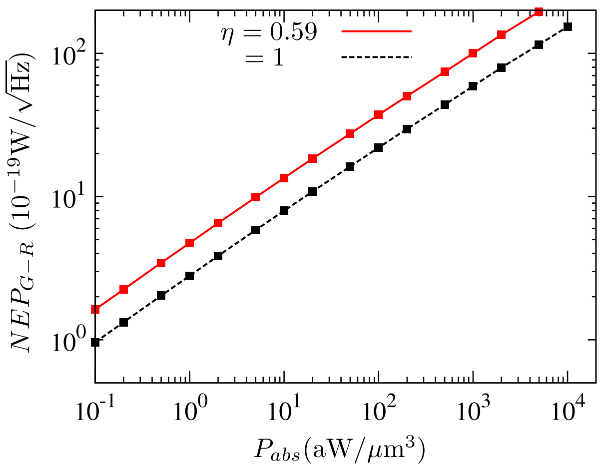

Figure 8. The effect of absorbed power on generation–recombination limited NEP for 2 values of signal detection efficiency η, resonator volume $V = 1000$ μm^3 and $\tau_l/\tau_{\mathrm{pb}} = 1$.

by quasiparticle scattering. For $P_{\mathrm{abs}} \to 0$ we find $\eta_{2\Delta} \to 0.6$ which interestingly is the result found for high-energy interactions $h\nu \gg 2\Delta$. Figure 6(d) shows that τ_r is reduced as P_{abs} is increased and, as expected, mirrors the increase in N_{qp}. The full curve in (d) is the distribution-averaged *thermal* recombination time at T^*_{N}, $\langle\tau_r(T^*_{\mathrm{N}})\rangle_{\mathrm{qp}}$, which gives a very good description of the recombination time of the driven $f(E)$ typically within a few percentage. The deviation increases with P_{abs} which again is expected: the distortion of $f(E)$ with P_{abs} from the T^*_{N} distribution increases the available final phonon densities of states for recombination.

Figure 7 shows (full lines) calculated $|S_{21}|^2$ for the driven $f(E)$ for absorbed powers: (a) $P_{\mathrm{abs}} = 0$ at T_{b}, (b) $P_{\mathrm{abs}} = 0.1$ aW μm^{-3}, (c) $P_{\mathrm{abs}} = 2$ aW μm^{-3} and (d) $P_{\mathrm{abs}} = 50$ aW μm^{-3}. The dotted lines show $|S_{21}|^2$ for the nearest thermal distribution $f(E, T^*_{21})$ giving the same ν_0 in each case. Note here that S_{21} is sensitive to the value of the gap used in calculating σ so that the energy gaps used are the self-consistent gaps calculated using equation (3). A general characteristic of all calculated transmission curves is that the driven S_{21} has a higher Q (it is deeper and narrower) than the nearest T^*_{21} prediction. This arises due to occupation of final states for absorption by the driven distributions. For increasing P_{abs} the divergence increases. This is a further effect of the increasing distortion of $f(E)$ as a function of P_{abs} observed in relation to figure 2. The inset shows that T^*_{N} gives a reasonable account of T^*_{21} for the range of P_{abs} considered, particularly at low powers.

The intrinsic limiting NEP of a superconducting detector in thermal equilibrium is determined by the random generation and recombination of quasiparticles [27]. In thermal equilibrium $\mathrm{NEP_{G\text{–}R}} = 2\Delta/\eta\sqrt{N_{\mathrm{qp}}V/\tau^*_r}$ where η is the fraction of *detected* power P_{det} coupling to the quasiparticles, V is the volume of the SR, and the effective recombination time $\tau^*_r = \tau_r\left[1 + \tau_l/\tau_{\mathrm{pb}}\right]/2$. Here the factor of two arises because, as noted by Kaplan *et al* and others, τ_r is the recombination time of a single quasiparticle whereas two quasiparticles are lost in each event [23, 28, 29]. For detection of high-energy photons $h\nu_\Phi \gg 2\Delta$, $\eta \simeq 0.59$ [14–16]. If we assume that $P_{\mathrm{det}} \ll P_{\mathrm{abs}}$ so that $\delta N_{\mathrm{qp}}/N_{\mathrm{qp}}$ is small (as it must be for a linear detector) then the relevant N_{qp} and τ_r are as already calculated. Figure 8 shows $\mathrm{NEP_{G\text{–}R}}$ as a function of P_{abs} for a SR with $V = 1000$ μm^3 and $\tau_l/\tau_{\mathrm{pb}} = 1$ for 2 values of η, and we have assumed that the equilibrium expression for $\mathrm{NEP_{G\text{–}R}}$ applies for the driven case. P_{abs} determines the limiting NEP and even for the lowest P_{abs} studied, $\mathrm{NEP_{G\text{–}R}} \sim$ 1–5 $\times$ 10^{-19} W Hz$^{-1/2}$.

7. Analytical power model

The preceding calculations provide insight into the effects of P_{abs} with $\nu_{\mathrm{p}} \ll 2\Delta/h$ at low reduced temperatures on low-T_{c} SRs. However in many situations, for example for estimates of performance or for extrapolation to other materials, an expression to approximate the key results would be extremely powerful. Recombination determines the overall time-evolution of the driven system, even though we have shown that only a power-dependent fraction $\eta_{2\Delta}$ of P_{abs} is carried by the recombination phonons. An approximate equation giving an estimate of T^*_{N} as a function of P_{abs} can be derived considering energy conservation so that

$$\int_0^{P_{\mathrm{abs}}} \mathrm{d}P\, \eta_{2\Delta} = \int_{T_{\mathrm{b}}}^{T^*} \mathrm{d}T\, \frac{C_{\mathrm{BCS}}(T)}{\langle\tau_r(T)^*\rangle_{\mathrm{qp}}}, \tag{12}$$

where the denominator on the right-hand-side is the distribution-averaged effective thermal recombination time and $\tau^*_r(T) = \tau_r(T)\left[1 + \tau_l/\tau_{\mathrm{pb}}\right]/2$. C_{BCS} is the BCS specific heat capacity which comprises two terms [30]. The first is the quasiparticle heat capacity $C_{\mathrm{qp}} = 4N(0)\mathrm{d}/\mathrm{d}T(\int_\Delta^\infty \mathrm{d}E\, Ef(E)\, \rho(E))$ and the second arises because the quasiparticle energies E themselves change due to their dependence on Δ. At the (effective) temperatures considered here $\mathrm{d}\Delta/\mathrm{d}T \simeq 0$. The data of figure 6(c) were fitted to a log-linear model giving $\eta_{2\Delta} = -0.03\ln(P_{\rm abs}/{\rm aW}\ \mu{\rm m}^{-3}) + 0.384$. At very low absorbed powers $P \to 0$ we find $\eta_{2\Delta} \to 0.6$. With the same limit equation (12) was solved. The result is shown as the full line in figure 6(b). The account of $T_{\rm N}^*$ as a function of $P_{\rm abs}$ is very satisfactory.

We found that the functional form of $T_{\rm N}^*$ with $P_{\rm abs}$ can be further approximated by the simpler expression

$$P_{\rm abs} = \frac{1}{\eta_{2\Delta(P_{\rm abs})}}\Sigma_s\left(\frac{1}{1+\tau_l/\tau_{\rm pb}}\right) \times \left[T_{\rm N}^*\exp\left(\frac{-2\Delta(T_{\rm N}^*)}{k_{\rm b}T_{\rm N}^*}\right) - T_{\rm b}\exp\left(\frac{-2\Delta(T_{\rm b})}{k_{\rm b}T_{\rm b}}\right)\right]. \quad (13)$$

where $\eta_{2\Delta(P_{\rm abs})}$ is the fraction of power carried by 2Δ-phonons at $P_{\rm abs}$. For the Al film modeled here we found $\Sigma_s = 3.4\times10^{10}$ W m^{-3} K^{-1}. This function is indistinguishable from the full curve plotted in figure 6(b) and gives a good account of the effect of $P_{\rm abs}$ on $T_{\rm N}^*$ for the parameter space studied. Both equations (12) and (13) provide a straightforward route to estimate $N_{\rm qp}$ and τ_r as a function of $P_{\rm abs}$.

8. Discussion and conclusions

We have calculated the non-equilibrium distributions of quasiparticles and phonons, $f(E)$, $n(\Omega)$ generated by a flux of low-energy photons $h\nu_{\rm p} \ll 2\Delta$ as a function of $P_{\rm abs}$ for a thin-film superconducting resonator at low temperatures $T/T_{\rm c} = 0.1$. Driven $f(E)$ deviate from thermal-like distributions exhibiting structures associated with multiple probe-photon absorption and emission for all $P_{\rm abs}$ studied. All calculated $n(\Omega)$ show pair-breaking phonons $\Omega \geq 2\Delta$ for all $P_{\rm abs}$ studied. The density of driven quasiparticles exceeds their thermal density at the bath temperature, confirming a simple estimate based on energy conservation using thermal scattering times. The driven $f(E)$ can be characterized in terms of an effective temperature $T_{\rm N}^*$ which also gives a good account of the distribution averaged, *driven* recombination time τ_r and this can be very-well approximated using simpler expressions to calculate the *thermal* recombination time at $T_{\rm N}^*$. Using $N_{\rm qp}$ and τ_r a (dark) detector Noise Equivalent Power can be calculated. We find that dissipation limits the achievable NEP in the range of $P_{\rm abs}$ considered indicating a minimum NEP $\sim 1\times10^{-19}$ W Hz$^{-1/2}$ although we emphasize this depends on the actual absorbed power.

Reference [6] measured a $\lambda/2$ Al resonator where we expect out-diffusion should be minimized. That work estimated a limiting effective quasiparticle temperature of order 160 mK with $T_{\rm b} = 100$ mK, $N_{\rm qp} \sim 20$–$70\ \mu{\rm m}^{-3}$, $\tau_r \sim 3.5$–0.5 ms depending on the power, and a dark NEP $\sim 2\times10^{-19}$ W Hz$^{-1/2}$ at the lowest probe power. Quantifying $P_{\rm abs}$ from the reported results is difficult without knowing details of the embedding circuit. However our calculations shown in figures 6(a), (b) and (d) indicate these densities, temperatures, and lifetimes would arise for $P_{\rm abs}$ in the range 0.1–1 aW μm^{-3}. For the same absorbed powers, figure 8 indicates a limiting dark NEP of 2–3 $\times 10^{-19}$ W Hz$^{-1/2}$. The agreement with our calculations, without free parameters, is extremely satisfactory whilst suggesting that the approach that we have described has merit.

In future work we will incorporate a pair-breaking source in the kinetic equations in addition to the probe signal. We will also investigate the effect of the probe frequency on the driven solutions, its effect on the achievable NEP, and the scaling of $\eta_{2\Delta}$ with material parameters. It will also be possible to model the detection of sub-gap photons $h\nu_\Phi < 2\Delta$ using a driven resonator.

References

[1] Day P K, LeDuc H G, Mazin B A, Vayonakis A and Zmuidzinas J 2003 A broadband superconducting detector suitable for use in large arrays *Nature* **425** 817–21
[2] Zmuidzinas J 2012 Superconducting microresonators: physics and applications *Annu. Rev. Condens. Matter Phys.* **3** 169–214
[3] Vardulakis G, Withington S and Goldie D J 2008 Superconducting kinetic inductance detectors for astrophysics *Meas. Sci. Technol.* **19** 015509
[4] Monfardini A *et al* 2010 NIKA: a millimeter-wave kinetic inductance camera *Astron. Astrophys.* **521** A29
[5] Baselmans J J A 2011 Kinetic inductance detectors *J. Low Temp. Phys.* **167** 292–304
[6] de Visser P J, Baselmans J J A, Yates S J C, Diener P, Endo A and Klapwijk T M 2012 Microwave-induced excess quasiparticles in superconducting resonators measured through correlated conductivity fluctuations *Appl. Phys. Lett.* **100** 162601
[7] DiCarlo L, Reed M D, Sun L, Johnson B R, Chow J M, Gambetta J M, Frunzio L, Girvin S M, Devoret M H and Schoelkopf R J 2010 Preparation and measurement of three-qubit entanglement in a superconducting circuit *Nature* **467** 575–8
[8] Hofheinz M, Weig E M, Ansmann M, Bialczak R C, Lucero E, Neeley M, O'Connell A D, Wang H, Martinis J M and Cleland A N 2008 Generation of Fock states in a superconducting quantum circuit *Nature* **454** 310–4
[9] Schoelkopf R V and Girvin S M 2008 Wiring up quantum systems *Nature* **451** 664–9
[10] Irwin K D and Lehnert K W 2004 Microwave SQUID multiplexer *Appl. Phys. Lett.* **85** 2107–9
[11] Bardeen J, Rickayzen G and Tewordt L 1959 Theory of the thermal conductivity of superconductors *Phys. Rev.* **113** 982–94
[12] Chang J J and Scalapino D J 1977 Kinetic-equation approach to superconductivity *Phys. Rev.* B **15** 2651–70
[13] Chang J J and Scalapino D J 1978 Nonequilibrium superconductivity *J. Low Temp. Phys.* **31** 1–32
[14] Zehnder A 1995 Response of superconducting films to localized energy deposition *Phys. Rev.* B **52** 12858–66
[15] Ishibashi K, Takeno K, Nagae T and Matsumoto Y 1991 Output signal from Nb-based tunnel junctions by irradiation of 6 keV x-rays *IEEE Trans. Magn.* **27** 2661–4
[16] Kurakado M 1982 Possibility of high resolution detectors using superconducting tunnel junctions *Nucl. Instrum. Methods* **196** 275–7
[17] Lenander M *et al* 2011 Measurement of energy decay in superconducting qubits from nonequilibrium quasiparticles *Phys. Rev.* B **84** 024501
[18] Martinis J M, Ansmann M and Aumentado J 2009 Energy decay in superconducting Josephson-junction qubits from nonequilibrium quasiparticle excitations *Phys. Rev. Lett.* **103** 097002

[19] Mattis D C and Bardeen J 1958 Theory of the anomalous skin effect in normal and superconducting metals *Phys. Rev.* **111** 412–7

[20] Doyle S, Mauskopf P D, Zhang J, Montfardini A, Swenson L, Baselsmans J J A, Yates S J C, Houwman E P and Roesch M 2010 A review of the lumped element kinetic inductance detector *Proc. SPIE* **7741** 77410m

[21] de Visser P J, Withington S and Goldie D J 2010 Readout-power heating and hysteretic switching between thermal quasiparticle states in kinetic inductance detectors *J. Appl. Phys.* **108** 114504

[22] Thompson S J, Withington S and Goldie D J 2012 Dynamical behaviour of superconducting resonators under readout-frequency, readout-power and signal-power switching *Proc. SPIE* **8452** 84520N

[23] Kaplan S B, Chi C C, Langenberg D N, Chang J J, Jafarey S and Scalapino D J 1976 Quasiparticle and phonon lifetimes in superconductors *Phys. Rev.* B **14** 4854–73

[24] Kaplan S B 1979 Acoustic matching of superconducting films to substrates *J. Low Temp. Phys.* **37** 343–65

[25] Eliashberg G M 1972 Inelastic electron collisions and nonequilibrium stationary states in superconductors *Sov. Phys.—JETP* **34** 668–76

[26] Ivlev B I, Lisitsyn S G and Eliashberg G M 1973 Nonequilibrium excitations in superconductors in high-frequency fields *J. Low Temp. Phys.* **10** 449–68

[27] Wilson C M, Frunzio L and Prober D E 2001 Time-resolved measurements of thermodynamic fluctuations of the particle number in a nondegenerate fermi gas *Phys. Rev. Lett.* **87** 067004

[28] de Korte P A J, van den Berg M L, Bruijn M P, Frericks M, le Grand J B, Gijsbertsen J G, Houwman E P and Flokstra J 1992 Superconducting tunnel junctions for x-ray spectroscopy *Proc. SPIE* **1743** 24

[29] Wilson C M and Prober D E 2004 Quasiparticle number fluctuations in superconductors *Phys. Rev.* B **69** 094524

[30] Tinkham M 1996 *Introduction to Superconductivity* 2nd edn (New York: McGraw-Hill)